Red Emitting Photonic Devices Using InGaP/InGaAlP Material System

by

Yamini Kangude

Submitted to the Department of Materials Science and Engineering and the Department of Electrical Engineering and Computer Science in partial fulfillment of the requirements for the degrees of

Master of Science in Materials Science and Engineering

and

Master of Science in Electrical Engineering and Computer Science

at the

MASSACHUSETTS INSTITUTE OF TECHNOLOGY

May 2005 [June 2005]

Author .....
Department of Materials Science and Engineering
May 20, 2005

Certified by .....
Leslie A. Kolodziejski
Professor of Electrical Engineering
Thesis Supervisor

Certified by .....
Yoel Fink
Professor of Materials Science and Engineering
Thesis Reader

Accepted by .....
Gerbrand Ceder, R.P Simmons Professor of Materials Science and Engineering
Chairman, Department Committee on Graduate Students
Department of Materials Science and Engineering

Accepted by .....
Arthur C. Smith
Chairman, Department Committee on Graduate Students
Department of Electrical Engineering and Computer Science

Red Emitting Photonic Devices Using InGaP/InGaAlP Material System

by

Yamini Kangude

Submitted to the Department of Materials Science and Engineering
and the Department of Electrical Engineering and Computer Science
on May 20, 2005, in partial fulfillment of the
requirements for the degrees of
Master of Science in Materials Science and Engineering
and
Master of Science in Electrical Engineering and Computer Science

Abstract

In this thesis, two red emitting photonic devices are presented using the InGaP/InGaAlP material system. InGaP/InGaAlP material system provides large flexibility in the band gap energy while being lattice matched to GaAs substrate. The devices consist of a quantum well active region and a distributed bragg reflector at the bottom to reduce loss of emitted light into the substrate. The first device emits at a wavelength of 650 nm and is intended to create a photonic crystal light emitting diode (PCLED). PCLEDs have been demonstrated to have higher efficiency compared to devices without the photonic crystal. The second device emits at 690 nm and is intended for integrating with an organic semiconductor to form a hybrid organic-inorganic emitter. The devices were grown using gas source molecular beam epitaxy (GSMBE) and then processed to form the final device.

Thesis Supervisor: Leslie A. Kolodziejski
Professor of Electrical Engineering

Thesis Reader: Yoel Fink
Professor of Materials Science and Engineering

Acknowledgments

This thesis has been possible due to the support and guidance of several people whom I would like to thank here individually.

First and foremost I would like to thank my thesis advisor, Prof. Leslie Kolodziejski, for her guidance thoughout the course of this thesis. When I had joined her group I knew little about photonics, but her door was always open for any kind of help, suggestions and feedback about the thesis work. I would also like to thank my thesis reader Prof. Yoel Fink for taking the time to read my thesis and offer valuable comments and suggestions.

I would like to thank Dr. Gale Petrich from the CBE group for his guidance and help at every step of my thesis work. I have bothered him the most with my constant queries and he always answered them happily. I would also like to thank the other members of the CBE group. Special thanks to Solomon (who has now graduated from the group) for training me on various fabrication techniques and also for his guidance in my graduate study at MIT. Thanks to my office-mate Sarah for the interesting discussions and to Sheila Tandon, Ryan Williams, Alexandra Markina and Reggie Bryant for their help whenever required.

A special thanks to my friend Vijay for pushing me when I needed it most, for motivating me and just being there with me always.

Finally I would like to thank my family for their love and support, especially my brother Shantanu for constantly showing me the right direction.

Contents

List of Figures

List of Tables

Chapter 1

Introduction

Semiconductor photon sources find applications in a wide variety of places. Besides display and other lighting applications, they are used in fiber-optic communication systems, optical data storage systems and also in scanning, reading and printing systems. They also offer several advantages over conventional lighting including reduced power consumption, compactness, durability and safety. Unlike incandescent or fluorescent lighting, semiconductor emitters create light with virtually no heat. Light emitting diodes (LEDs) prove to be very effective in applications where brightness, visibility and long-life are important. Red emitters find particular application in plastic optical fiber (POF) communication, since POF has an absorption minimum at 650 nm. Semiconductor photon sources are also desired for optical data recording in recordable DVDs.

Unfortunately, not all the light generated within a semiconductor LED is extracted out. A significant portion of the light is lost due to total internal reflection in the active region resulting in poor extraction efficiency. Being able to make semiconductor light emitters with higher efficiencies and at low processing cost is the main challenge in the area of semiconductor light sources. Higher extraction efficiency has been demonstrated using a two dimensional photonic crystal on top of the active region for a 980nm emitter [1]. The same concept can be applied to fabricate a high efficiency red emitter. Processing costs can be lowered by the use of organic materials which also enable the fabrication of flexible and lightweight optoelectronic components [2]. Since

the organic layers are highly disordered organic emitters can be produced cheaply. In addition, there is a huge variety of organic compounds with wide variety of electrical and optical properties which can be utilized for various functions. Also, organic materials can be layered on the substrates without introducing any strain and thus the growth process need not be limited by constraints of lattice matching. But organic semiconductors exhibit inferior charge transport properties and low chemical stability compared to inorganic semiconductors [3]. Hence novel devices integrating organic and inorganic semiconductors are an interesting area of current research.

1.1 Light generation using semiconductors

Light emission from a semiconductor takes place by the recombination of electrons and holes. Photons are emitted with energy equal to the band gap of the semiconductor. Since at room temperature there is not enough concentration of excited electrons and holes to produce discernible radiation, external sources of energy are required to excite electron-hole pairs into higher energy levels, which then recombine spontaneously resulting in radiation. When the external energy is provided electrically, it is called electroluminescence, whereas when another light source is used to provide energy, the phenomenon is called photoluminescence. The ratio of energy released in the form of photons to the input energy determines the efficiency of the emitter. One way to obtain higher efficiencies is to increase the probability of electron-hole recombination by confining them in a narrow region of space. This is achieved by the use of quantum wells. A quantum well is an ultrathin layer of narrow band gap material sandwiched between two layers of wider band gap materials. The resulting energy-band discontinuity leads to confinement of charge carriers in the quantum well [4].

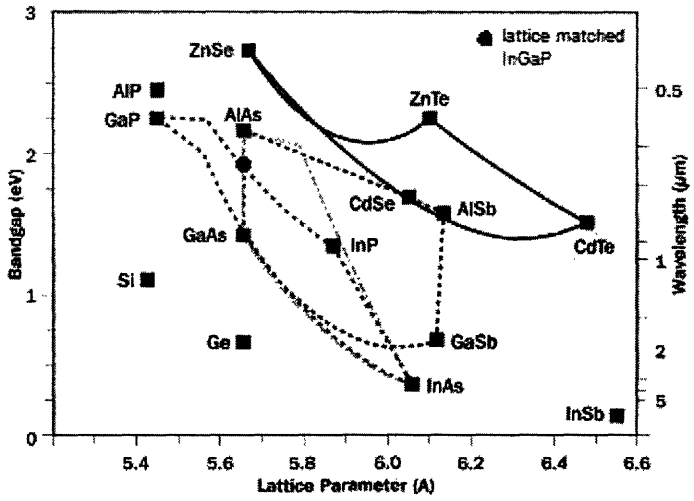

Figure 1-1: Band gap energy vs. lattice constant

1.2 InGaP-InGaAlP material system

The InGaP/InGaAlP material system is quite attractive by providing large flexibility in the band gap energy while being lattice-matched to a GaAs substrate. InGaAlP is an indirect semiconductor at certain Al content but can be used as a cladding layer for InGaP. Since the band gap of InGaAlP is higher than that of InGaP, there will be increased confinement of charge carriers in InGaP layer resulting in greater recombination rate and thus greater efficiency. Figure 1-1 shows a plot of the band gap energy versus the lattice constant of compound semiconductors. The figure shows that lattice-matched $In_{0.5}Ga_{0.5}P$ and $In_{0.5}Ga_xAl_{0.5-x}P$ layers can be grown on GaAs substrates. Since the lattice constant of GaP and AlP is same, any proportion of GaP and AlP can be mixed with each other without changing the lattice constant. Thus the composition of these alloys can be tailored to a specific emission wavelength as required. As seen from the diagram, the energy band gap includes the wavelength for red light (690nm). Besides, all the elements used in the InGaP/InGaAlP system are compatible. InP and GaP form solid solutions and do not segregate which makes the epitaxial growth of their ternary and quarternary alloys easy. Because of the above reasons, InGaP/InGaAlP material system can be utilized to make red emitting photonic devices emitting at the desired wavelengths.

1.3 Overview of thesis

In this thesis, two red emitting photonic devices are presented using the InGaP/InGaAlP material system. The first device is intended to create a photonic crystal light emitting diode (PCLED) that emits at a wavelength of 650 nm. PCLEDs have been demonstrated to have higher efficiency compared to devices without the photonic crystal [1]. The second device is a photonic emitter emitting at 690 nm and intended for integrating with an organic semiconductor to form a hybrid organic-inorganic emitter. The goal of the second device is to be able to pump J-aggregate cyanine dye, an organic semiconductor material which has an absorption peak at 690 nm. The devices were grown using gas source molecular beam epitaxy (GSMBE) and then processed to form the final device.

Chapter two describes the MBE system and the growth process of III-V semiconductor compounds. The various characterization techniques used for characterizing the devices are also presented in this chapter. These include photoluminescence measurements and X-ray diffraction and reflectivity measurements using a spectrophotometer.

Chapter three describes the design and fabrication steps for the two devices. Chapter three also describes the results of characterization of the devices using the techniques described in chapter two.

Chapter four discusses some of the issues in the design and fabrication of the devices and also the results of photoluminescence and reflectivity measurements on these devices.

Chapter five presents the conclusions and also some possibilities for future work on the devices described in this thesis.

Chapter 2

Experimental

The fabrication process of the devices involved growth of various semiconductor layers using Molecular Beam Epitaxy (MBE). The following section describes the MBE system used for epitaxial growth of these devices and the related process of epitaxial growth of compound semiconductors by Gas Source Molecular Beam Epitaxy (GSMBE). The devices were then characterized by Photoluminescence (PL), X-ray diffraction and reflectivity measurements which are described in the latter part of the chapter.

2.1 Molecular Beam Epitaxy

MBE was developed in the early 1970s as a means of depositing high-purity epitaxial layers of compound semiconductors. Since that time, MBE has evolved into a popular technique for depositing III-V compound semiconductors as well as several other materials. MBE can produce high-quality layers with very abrupt interfaces and good control of thickness, doping, and composition and is a valuable tool in the development of sophisticated electronic and optoelectronic devices. MBE provides high quality material which result in high internal quantum efficiency of optical sources.

2.1.1 MBE process

MBE is an epitaxial growth process involving the reaction of one or more thermal beams of atoms or molecules with a crystalline surface in a ultra high vacuum (UHV) environment [5]. Molecular beams of the constituent elements are generated from thermal Knudsen sources which interact on a heated crystalline substrate to produce a single crystal layer. The 'molecular beams' are typically generated from thermally evaporated elemental sources, but other sources include metal-organic group III precursors (MOMBE), gaseous group V hydride or organic precursors (gas-source MBE), or some combination (chemical beam epitaxy or CBE). The solid source materials are placed in evaporation cells to provide an angular distribution of atoms or molecules in a beam. The substrate is heated to the necessary temperature and, when needed, continuously rotated to improve the growth homogeneity. The temperature or flow of each source is set such that flux required to produce films of the desired composition may be obtained. Rotating the substrate improves the uniformity of the deposited film. The sources and the growth environment are surrounded by liquid nitrogen cooled cryo panels to minimize unintentional impurities in the deposited layers from the residual background [5]. To obtain high-purity layers, it is critical that the material sources be extremely pure and that the entire process occurs in an ultra-high vacuum environment. Another important feature is that growth rates are typically on the order of a few angstroms per second and the beams can be shuttered in a fraction of a second, allowing for nearly atomically abrupt transitions from one material to another.

Gas Source Molecular Beam Epitaxy is essentially conventional MBE with Group V elements supplied in the form of hydrides. The atomic beams of Group III elements are generated by heating an effusion cell. An effusion cell is an oven comprised of a ceramic Pyrolytic Boron Nitride (PBN) crucible surrounded by a heating coil. The solid elemental material is placed within the crucible. The effusion cells are heated to a temperature ranging from 750 degree C and 1200 degree C (depending on the material), at which point a molecular beam is generated via vaporization. The va-

porized material is blocked from the substrate surface by a molybdenum or tantalum shutter [6]. For growth, the shutter is opened for a time interval corresponding to the desired thickness of the material being deposited, with a simultaneous Group V flux being provided. The Group V elements are generated from the hydrides phosphine (PH_3) and arsine (AsH_3). The decomposition of the hydrides from MH_3 to M_2 and H_2 is accomplished by passing the hydride through cracker cells. A cracker is a high-temperature-low-pressure gas cell where the thermal decomposition (cracking) of the hydrides takes place. The cracker cell consists of a Pyrolytic Boron Nitride (PBN) tube followed by a high temperature zone containing high purity PBN chips. The thermal cracking takes place in the high temperature zone when the hydride is in contact with the PBN chips [7]. The temperature of the cracker ranges between 900 degree C and 1100 degree C. The rate at which the hydrides enter the cracker is accurately controlled by mass flow controllers (MFCs). In addition, the cracking efficiency of AsH_3 and PH_3 is nearly 100% for cracker temperatures between 900 and 1100 degree C. This makes the flux on the semiconductor surface precisely controlled [7]. MFCs also provide accurate and timely changes in hydride flow rates.

2.1.2 Basic Physical Processes

Each MBE arrangement can be divided into three zones where different physical phenomena take place. The first zone is the generation zone where molecular beams are generated under ultra high vacuum (UHV) conditions from the effusion cells. The temperatures of the effusion cells are accurately controlled by proportional-integral-derivative (PID) controllers. The beams from different sources intersect each other in the second zone. The vaporized elements mix together in the second zone called the mixing zone creating a special gas phase. The third zone is the substrate surface where crystallization takes place and hence is called the crystallization zone [8]. The surface processes taking place in the crystallization zone are as follows:

1. adsorption of constituent atoms or molecules impinging on the substrate surface,

2. surface migration and dissociation of the adsorbed molecules

3. incorporation of the constituent atoms into crystal lattice of the substrate or the epilayer already grown,

4. thermal desorption of the species not incorporated into the crystal lattice.

2.1.3 The GSMBE system

The GSMBE system used for deposition of layers in the devices presented in this thesis is a Instruments SA Riber 32P machine. The reactor is part of an integrated II-VI/III-V epitaxy system, shown in Figure 2-1. In the system, all chambers, both II-VI and III-V reactors, an Auger electron spectroscopy (AES) system, a sample bake out chamber, and an introduction chamber are connected in-situ by a transfer chamber. The base pressure of all systems is 5×10^{-9} Torr or lower. The Riber MBE system has solid aluminum, gallium and two indium sources as Group III sources. The Group V materials available are arsenic and phosphorous through the thermal decomposition of arsine and phosphine gas, and the dopant sources are solid silicon and beryllium. Silicon, beryllium and aluminum effusion cells are single filament, whereas the two indium cells and a gallium cell are dual filament cells. Ceramic inserts with an eight degree taper, have been added at the lip of each crucible in order to increase surface uniformity of the deposited material. The pumping systems on the GSMBE system are a Pfieffer 2200 l/s turbomolecular pump with an Edwards mechanical backing pump and a CTI cryopump (as a back up). The turbo pump is used in most cases, and always during growth, due to the high chamber pressures (10^{-5} Torr) that result from cracking the hydrides. This system also contains a hydrogen cracking cell supplied by EPI, for generation of atomic hydrogen for low temperature oxide removal techniques [9].

2.1.4 Procedures for MBE

This section describes a set of general procedures for growing films in an MBE system. The mounted substrate is introduced into the sample introduction chamber. The introduction chamber is evacuated at least to the millitorr range and preferably lower

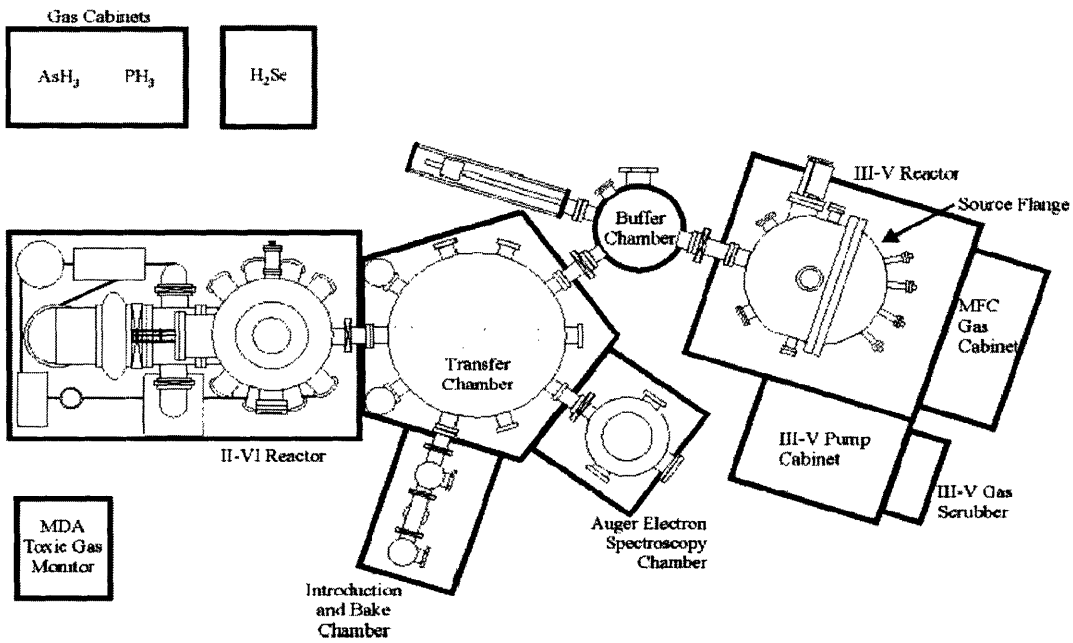

Figure 2-1: Riber 32P molecular beam epitaxy system and other interconnected ultrahigh vacuum chambers

before opening the intro chamber's gate valve. The sample is then moved into the transfer chamber in which a UHV environment is maintained. There the sample is heated to 210 degree C to remove any adsorbed water. After baking, the sample is then transported into the buffer chamber and attached to the 'Riber sample holder' [6]. Finally the sample is transferred into the Riber MBE reactor.

Before beginning the actual growth on the substrate, the solid sources to be used in a given deposition and the cracker cell are heated and allowed to stabilize at the temperature required to generate the necessary beam flux. All sources are covered by a shutter and the sample wafer is positioned out of the line of sight to prevent any material that might vaporize from depositing on the wafer. The substrate is also heated simultaneously to remove the native surface oxide. After the removal of the native oxide, the Group V beam flux and substrate temperature are adjusted to what is desired for the deposition. First, a buffer layer of the same composition as the substrate is grown. This is initiated by opening the shutters in front of the appropriate cells. In the normal mode of operation, a layer is terminated by shuttering

the Group III beams. For changing the Group V element, the switch over is done when no layer is growing. The 'switch over' takes about 5 to 15 seconds. The next layer is then grown by re-establishing the III fluxes as desired. After the growth of the epitaxial layers, the substrate heater is turned off. The sample is allowed to cool and then moved from the sample manipulator into the introduction chamber and removed from the system [6].

2.2 Characterization Techniques

2.2.1 Photoluminescence measurement

Photoluminescence (PL) is the optical emission obtained by photon excitation and is commonly observed with direct bandgap III-V semiconductor materials. A PL measurement involves exciting carriers with an incident beam of light of sufficient energy and recording the resulting emission intensity as a function of wavelength to produce an intensity spectrum. The intensity and spectral content of the resulting emission provides information on the quality of material properties of the sample. Photoluminescence is a direct measure of various important material properties.

In a PL measurement, a laser beam is focused on the sample where it is absorbed and results in excitation of electrons and holes to higher energy levels; this process is called 'photo-excitation'. When the excited electrons return to their equilibrium states, the excess energy is released via radiative processes in which light is released or via non-radiative processes which do not involve the emission of light. By creating a high quality, low defect concentration film, the proportion of energy released through light emission can be increased. The energy of the emitted light or photoluminescence is related to the difference in energy levels between the two electron states involved in the transition, or between the excited state and the equilibrium state. Thus, a peak in intensity is observed at the wavelength corresponding to the energy involved in the transition. The quantity of the emitted light is related to the relative contribution of the radiative process.

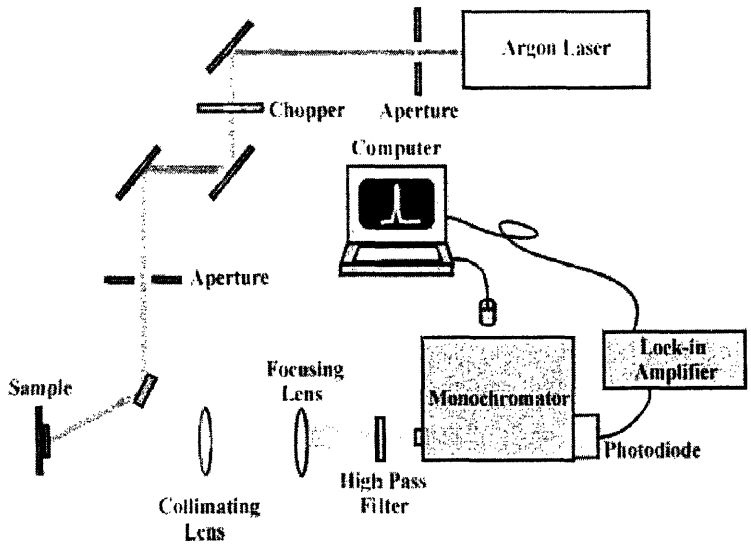

Figure 2-2: Schematic of PL measurement set up

Figure 2-2 shows the set up used for measuring room temperature PL. The sample is pumped using an Argon laser emitting at a wavelength of 488 nm. The emitted light first passes through a beam chopper which forms pulses of the light. These pulses then strike the sample where they are absorbed. The resulting radiation from the sample is focused into a spectrometer and is detected with a Si photomultiplier. The emitted light intensity is measured with a lock-in amplifier.

2.2.2 X-Ray Diffractometry

X-ray diffractometry is a very useful technique to determine material quality. X-ray diffractometry provides information about the composition, lattice matching and thickness of a semiconductor film. In this section, a brief overview of the diffraction theory and its implementation by high resolution x-ray diffractometry is presented. The triple axis diffractometer used for analysis of the layers is also described.

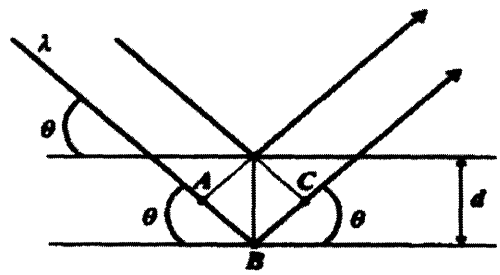

Figure 2-3: Geometric representation of Bragg's Law

X-ray diffraction theory

X-ray diffraction is a technique for establishing the structures of crystalline solids by directing X rays of a particular wavelength at a crystal and obtaining a diffraction pattern from which the lattice periodicity in the crystal can be determined. This phenomenon can be explained most simply by Bragg's law. Figure 2-3 shows its graphical representation. When a beam of x-rays strikes a crystal, the x-rays are scattered by the atomic planes of the crystal. When the angle of incidence is equal to angle of diffraction and the path difference between the scattered beams is an integer multiple of the wavelength of the x-ray used, strong diffraction occurs. The scattered beams constructively interfere and result in peaks of intensity. For the case shown in Figure 2-3, the path difference, ABC, must equal $n\lambda$. This diffraction condition is expressed in the form of the following equation which is also know as Bragg's law.

$$n\lambda = 2dsin\theta \tag{2.1}$$

In this equation, n is the integer representing the order of diffraction, λ is the wavelength used, d is the inter planar spacing of the reflecting (diffracting) plane and θ is the angle of incidence, and of diffraction, of the radiation relative to the reflecting plane. Thus the interplanar spacing can be found from the angle at which peaks of intensity are observed, using the above equation [10].

High resolution X-ray diffractometry

A rocking curve is the plot of intensity versus the diffraction angle for a sample. A plane wave rocking curve is used as a reference. Rocking curve is the curve that

would be obtained by measuring with a perfectly parallel, monochromatic incident beam. X-ray beam has both a wavelength spread and a divergence. In order to do an accurate analysis, the incident beam should be as close as possible to a plane wave, hence the wavelength spread and beam divergence should be minimized. This is accomplished by the use of a beam conditioner which is a further diffracting system before the specimen of interest. The measured rocking curve is now the correlation of the plane wave rocking curve of the beam conditioners and the specimen crystals. The diffracting characteristics of the specimen can be deduced from the rocking curve measurement. The simplest conditioner is a perfect crystal of the same type as the specimen, using the same reflecting planes but with the deviation of the diffracted beam in the opposite sense to that at the specimen [10].

Figure 2-4 shows a schematic of the high resolution triple axis x-ray instrument used here. The incident beam enters the conditioner which reduces the divergence and wavelength spread of the beam using a combination of diffracting elements and angular-limiting apertures. The resulting beam is then directed at the specimen. The specimen can be tilted so that the normal to the reflecting plane lies in the plane of the diagram. The diffracted beam then enters a detector through an analyser which restricts its angular acceptance. In the triple axis instrument, the differential movements of the beam conditioner, specimen and analyser make the measurement and determine the precision.

The X-ray characterization system

The system used for the x-ray characterization of the device layers was a *Bede* D^3 system. Figure 2-5 shows a diagram of this system. The system has two beam conditioners to reduce the wavelength spread and divergence of the incident beam. It has an (enhanced dynamic range) EDR detector which detects the diffracted beam. The angular accuracy that can be obtained using this instrument is 0.055 arcseconds on θ and 2θ axes. The design of the beam conditioners is described below.

Each crystal contains two channels cut into a single block of highly perfect silicon. The first channel is cut to give two asymmetric 022 Bragg reflections, increasing the

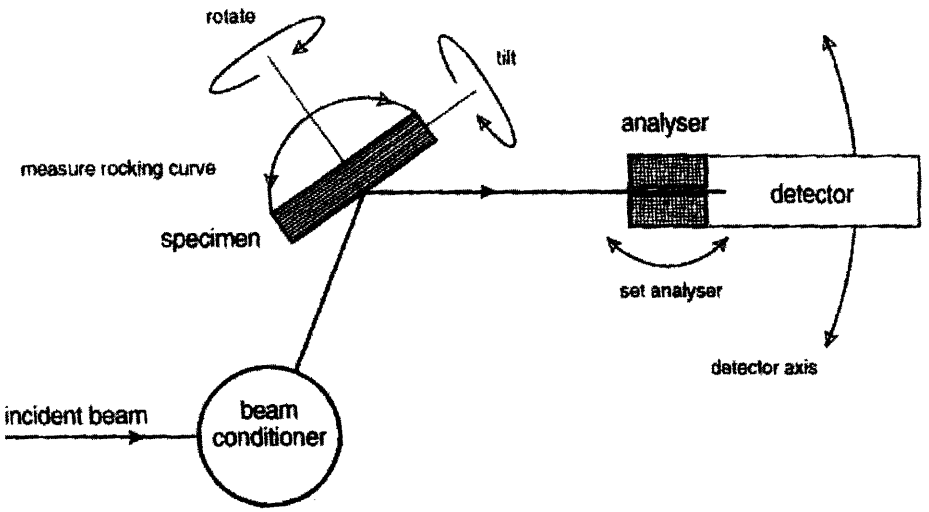

Figure 2-4: Schematic of high resolution triple axis instrument [10]

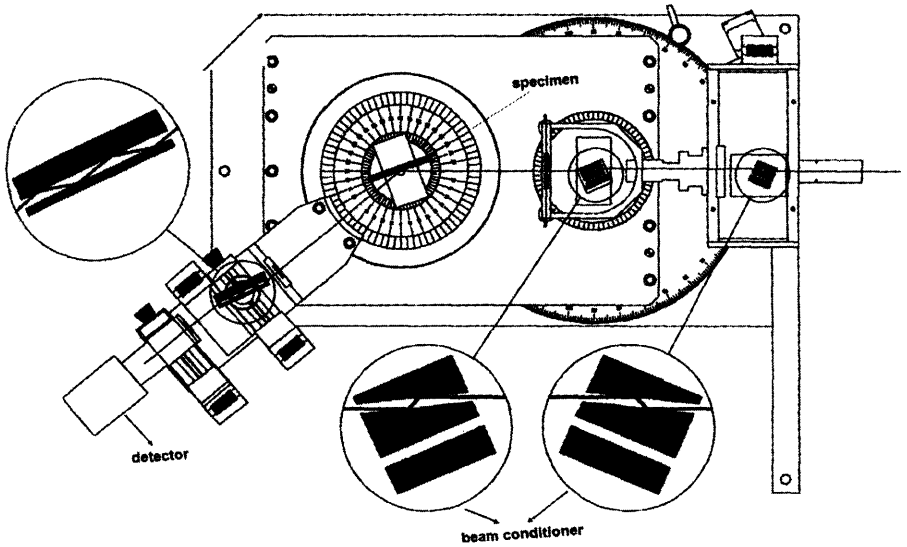

Figure 2-5: Diagram of high resolution triple axis instrument [11]

angular acceptance and providing high intensity. The second provides four symmetric 022 reflections for extremely high resolution work. Changing between the two channels is achieved by translating the crystal using computer control and no realignment of the crystal is necessary. The first beam conditioner, may be used individually to provide a high intensity beam for X-ray reflectivity, or withdrawn completely to allow a beam divergence slit to be used for single crystal and double crystal diffraction. The second conditioner is mounted on the first axis and used along with the first crystal to provide a high performance monochromator. The two crystals can be translated under computer to set the monochromator to either high intensity or high resolution mode. The wavelength can be set precisely to the $K\alpha 1$ line by rotating the second element.

2.2.3 Reflectance measurement using a spectrophotometer

Spectrophotometry is the quantitative measurement of the reflection or transmission properties of a material as a function of wavelength. Reflectance is measured by spectrophotometers by measuring the amount of light reflected by a surface as a function of wavelength and producing a reflectance spectrum. In a reflectance measurement, a beam of light from a light source is passed through a monochromator and then focused on the sample surface. The resulting reflected light is then analysed through a detector generating the reflectance spectrum.

The reflectance of the 'Bragg mirror' (to be discussed in Section 3.1.2) in our devices was measured using the Absolute Specular Reflectance accessory of the Cary 5E UV-Vis-NIR Dual-Beam Spectrophotometer. The Absolute Specular Reflectance accessory measures the 'mirror like' reflectance off a sample surface. The reflectance accessory is installed in the sample compartment of the spectrophotometer. The optical elements are mounted on a movable platform which can be lifted out and replaced by another accessory for other measurements.

Figure 2-6 shows the optical design of the specular reflectance accessory. This accessory features a dual 'VW' configuration as shown in Figure 2-6 and consists of one spherical mirror and two toroidal mirrors per beam. The spherical mirror is movable

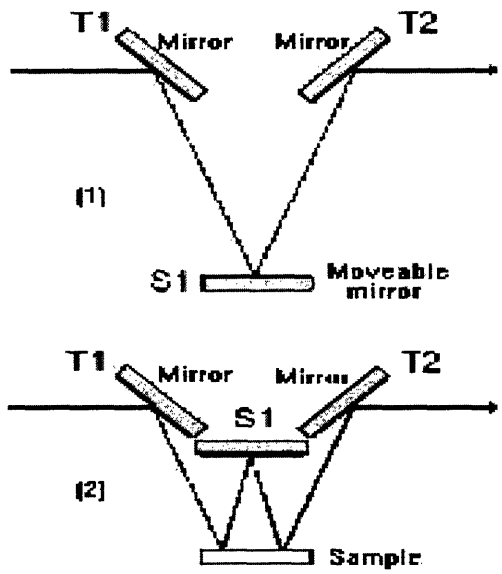

Figure 2-6: Optical design of the specular reflectance accessory: (1) shows the V path configuration for calibration. (2) shows the W path configuration for measurements. [12]

allowing the use of the same mirror for both calibration and sample measurement. During calibration both the reference and the sample beams are configured in the 'V' path. In the calibration or 100% reflectance position, the light from the monochromator, of intensity I strikes the toroidal mirror T1, which has a reflectivity of RT1, and reflects onto the movable spherical mirror S1. This then reflects the beam with a reflectivity of RS1 onto the second toroidal mirror T2, which has a reflectivity of RT2. The beam is then focused onto the detector optics. This completes the 'V' path. The spectrophotometer reads the ratio:

$$R100 = (I(RT1)(RS1)(RT2))/(I'(RT1')(RS1')(RT2')) \tag{2.2}$$

where the primed values refer to the reference beam. During the measurement, the sample beam is configured in the 'W' path while the reference beam is still in the 'V' position. The 'W' path is formed by placing the sample of reflectivity Rr in place and moving the spherical mirror S1 to the new position as shown in the figure. The beam from T1 is intercepted by the sample and reflected onto S1. S1 reflects the beam back onto the sample a second time, and from there onto T2, and onto the detector. This

double bounce off the sample forms the 'W' path. The sample reflectance is given from the ratio:

$$Rsample = (I(RT1)(Rr)(RS1)(Rr)(RT2))/(I'(RT1')(RS1')(RT2')) = (Rr^2)(R100) \tag{2.3}$$

As R100 was set to read 100% reflectance, the ratio Rsample is reduced to Rr^2. Thus Rsample gives the square of the absolute specular reflectance of the sample [12].

The light source used in this instrument is a tungsten halide lamp and a photomultiplier tube is used as a detector. The wavelength range is from 175 nm to 3300 nm. The angle of incidence is 7 degrees to normal. By using the same optical elements for both calibration and sample measurement, a truly absolute reflectance measurement may be attained [12].

Chapter 3

Results

The design, fabrication steps and results of characterization of the devices are described in this chapter.

3.1 Design

The device structure consists of two parts: an active region where light is generated and a Bragg mirror between the active region and the substrate. The design of both the active region and the mirror is described in detail below.

3.1.1 Active Region

The active region design consists of a quantum well enclosed by two cladding layers. A quantum well structure is chosen for the active region as it results in carrier confinement. As a result of confinement of electrons and holes to the same narrow region, the probability of recombination of electrons and holes increases. A greater percentage of recombination in turn leads to a greater amount of light emitted for the same input power resulting in higher efficiencies. The quantum well is made of InGaP as its band gap energy lies in the red region of the electromagnetic spectrum. InGaP is also a direct band gap semiconductor and thus emits light without generating any heat. The cladding layers should have higher band gap than the quantum well layer.

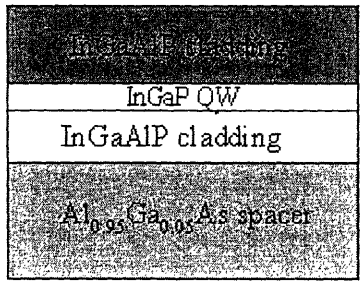

Figure 3-1: Schematic of the 650 nm structure

Hence InGaAlP is chosen for the cladding layer.

Two emitter structures were grown: the first was intended to emit at a wavelength of 650 nm and the second to emit at a wavelength of 690 nm. The details of the individual designs are described below.

650 nm emitter design

The active region of the device emitting at 650 nm was made of $In_{0.5}Ga_{0.5}P$ quantum well and $In_{0.5}Ga_{0.15}Al_{0.35}P$ cladding layers. $In_{0.5}Ga_{0.5}P$ and $In_{0.5}Ga_{0.15}Al_{0.35}P$ are both lattice-matched to GaAs, thus growth of these layers on GaAs does not produce any strain. The thickness of the quantum well was determined based on the results of PL of a structure consisting of two quantum wells with varying thickness. One of the quantum wells was 2 nm thick and the other was 6 nm thick. PL measurements showed only the peak due to 6 nm thick quantum well at room temperature, hence 6 nm was chosen as the thickness for the quantum well. The lower cladding layer was made 30 nm thick. The upper cladding layer was made much thicker (150 nm) than the lower layer with the intention of etching a photonic crystal in that layer. The structure was grown on top of a 500 nm thick $Al_{0.95}Ga_{0.05}As$ spacer layer. Figure 3-1 shows the schematic of the 650 nm emitter structure.

690 nm emitter design

A multi-quantum well structure was used for the active region of the device emitting at 690 nm to increase the amount of light emitted. Multi-quantum wells increase the

number of carrier recombination sites and thus further enhance the efficiency of the emitter. The structure was made of three quantum wells of $In_{0.62}Ga_{0.38}P$ enclosed by $In_{0.5}Ga_{0.15}Al_{0.35}P$ cladding layers. The quantum wells were 8 nm thick and the cladding layers were 30nm thick. The composition of the quantum well was changed from that used for the 650 nm emitter to shift the wavelength of emission of the device. The percentage of InP to GaP was increased in these quantum wells as InP has a smaller band gap compared to GaP and would result in decrease in the band gap energy of the ternary semiconductor. A smaller band gap energy will result in longer wavelength thus shifting the wavelength from 650 to 690 nm. The quantum wells were separated by a 5 nm barrier layer of $In_{0.5}Ga_{0.28}Al_{0.22}P$.

3.1.2 The Distributed Bragg Reflector

The active region is grown on top of a distributed bragg reflector (DBR) so as to prevent loss of emitted light into the underlying substrate. The DBR would reflect downward propagating light from the active region into the upward direction and thus avoid absorption of light by the substrate. The DBR consists of alternating layers of high and low dielectric materials of quarter wavelength thickness. The thickness and composition of the layers is chosen such that this arrangement strongly reflects light at normal or near normal incidence. Thus any light emitted from the quantum wells and directed into the substrate will be reflected back by the DBR increasing the extraction efficiency. Two different DBR designs are presented in this thesis. The first DBR consists of an oxide layer and hence requires an extra oxidation step during the fabrication process. The second DBR was designed to avoid the extra oxidation process and hence was designed without the oxide layer. The two DBR designs are described below.

Oxidized DBR

The first DBR was designed to reflect strongly at a wavelength of 650 nm. The DBR was made of seven bilayers of $InGaAlP/Al_xO_y$. Al_xO_y was formed by oxidation of

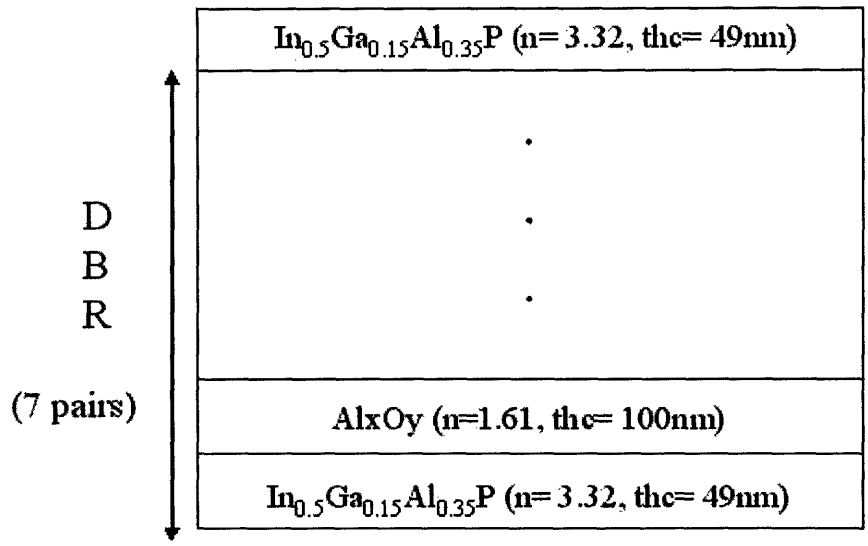

Figure 3-2: Schematic of the InGaAlP/AlxOy DBR

AlAs layers. $In_{0.5}Ga_{0.15}Al_{0.35}P$ has a dielectric constant of 3.32 at 650 nm and forms the high dielectric constant layer in the DBR. Al_xO_y has a dielectric constant of 1.61 at 650 nm and forms the low dielectric constant layer. The thickness of each layer is given by a quarter-wave ($t = 650/4n_{layer}$). This results in maximum reflectivity from the DBR. From the above calculation, the thickness of Al_xO_y layers was found to be 100nm and that of $In_{0.5}Ga_{0.15}Al_{0.35}P$ layers to be 49nm. Figure 3-2 shows the schematic of the oxide DBR and its calculated reflectance is shown in Figure 3-3.

Non-oxidized DBR

The second DBR consists of alternating layers of AlGaAs and AlAs and is designed to reflect strongly at 690 nm. $Al_{0.4}Ga_{0.6}As$ was used as the high dielectric constant layer and AlAs was used as the low dielectric constant layer for the DBR. Since the dielectric contrast between $Al_{0.4}Ga_{0.6}As$ and AlAs is not very high, a greater number of bilayers are required for this design. Sixteen bilayers of AlAs/AlGaAs were grown to provide strong reflectivity. The complete 690 nm emitting device consisted of the multi-quantum well structure presented in section 3.1.1. grown on top of the AlAs/AlGaAs DBR. The entire structure is grown on a 2 inch diameter

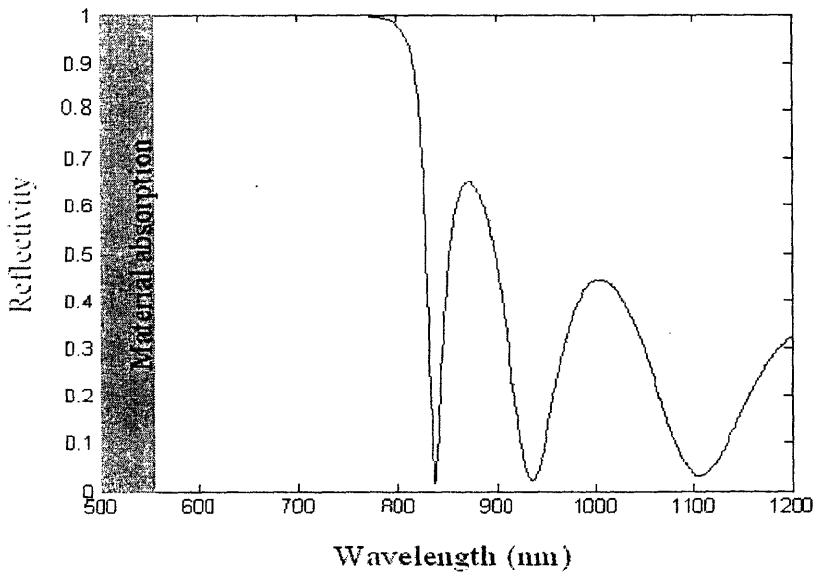

Figure 3-3: Calculated reflectance for InGaAlP/AlxOy DBR

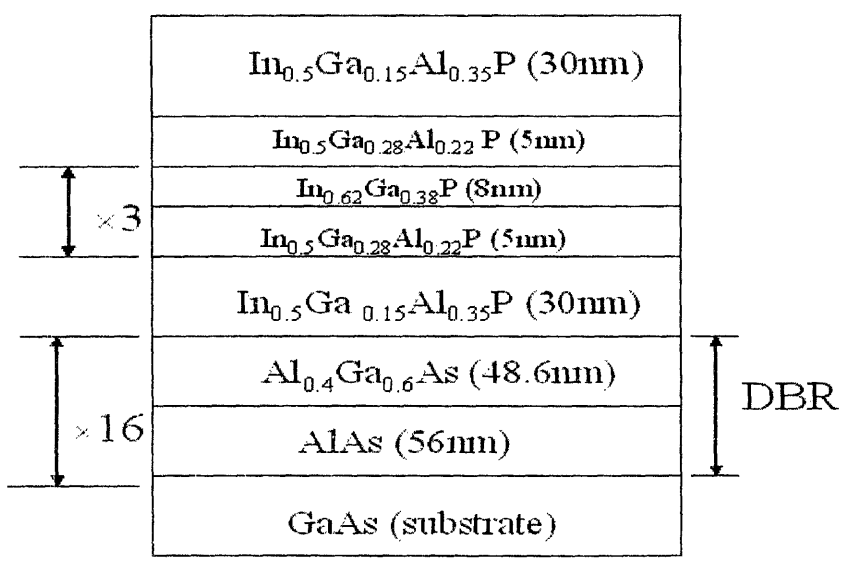

Figure 3-4: Schematic of the 690 nm emitter structure including both the active region and the DBR

Layer	$T_{substrate}$ (degree C)	Phosphine Flow Rate (SCCM)	Arsine Flow Rate (SCCM)	Growth Rate (nm/min)
$In_{0.62}Ga_{0.38}P$	477	2	-	7.5
$In_{0.5}Ga_{0.28}Al_{0.22}P$	480	2	-	11.9
$In_{0.5}Ga_{0.15}Al_{0.35}P$	483	2	-	10.3
$Al_{0.4}Ga_{0.6}As$	601	-	1	17.6
AlAs	601	-	1	7.2

Table 3.1: Growth conditions for the layers in the 690 nm emitter structure

GaAs substrate. A schematic of the 690 nm emitter structure including the active region and the DBR is shown in Figure 3-4.

3.2 Fabrication

3.2.1 MBE growth

The device structure for the 690 nm emitter is grown using gas-source molecular beam epitaxy (GSMBE) in a Riber 32P system. The growth process using GSMBE and the GSMBE system are described in section 2.1. The growth conditions for the final device structure were obtained by growing test structures with just the quantum wells or the DBR only. All the structures were grown on GaAs substrates. The growth conditions used during the growth of the 690 nm emitter are listed in Table3.1.

After the growth of the DBR layers, the substrate temperature was reduced to 470 degree C in fifteen minutes and the Gallium and Indium cell temperatures were adjusted to the values required for the cladding layer growth. Similarly when switching from the cladding layer to the barrier layer and vice versa, a 1.5 minute ramp time was used to adjust the Ga and In cell temperatures to the new values.

The growth details of the 650 nm structure are listed in Table 3.2.

Layer	$T_{substrate}$ (degree C)	Phosphine Flow Rate (SCCM)	Arsine Flow Rate (SCCM)	Growth Rate (nm/min)
$In_{0.5}Ga_{0.5}P$	470	2	-	7.5
$In_{0.5}Ga_{0.15}Al_{0.35}P$	470	2	-	10.3
$Al_{0.95}Ga_{0.05}As$	640	-	1	17.6

Table 3.2: Growth conditions for the layers in the 650 nm emitter structure

3.2.2 Patterning

The oxidation process for the formation of Al_xO_y layers in the DBR involves diffusion of oxygen into the structure from an exposed edge and hence oxidation of the entire wafer would take a very long time. Therefore, the wafer containing the device structure was patterned into circular mesas of 500 microns diameter which can be oxidized much faster than oxidizing the whole wafer. The first step in the patterning process was the deposition of a SiO_2 layer by sputtering that can be used as a hard mask for etching. The sample was sputtered for 30 minutes to form an approximately 100 nm thick SiO_2 layer. Next a pattern of circular mesas is transferred onto the SiO_2 layer by photo-lithography. A mask containing circles with 500 microns diameter and spaced by 700 microns is used for patterning. The patterning process involves first spinning on a drop of photoresist on the sample and exposing in UV light through the above mentioned mask. A Shipley 1813 positive resist is used and is spun at a rate of 4000 rpm for 30 seconds resulting in a 1.3 micron thick layer. The exposed sample is then developed using a developer solution which removes the exposed regions of the photoresist resulting in the transfer of the circular pattern on the mask to the resist. The pattern obtained in the resist is then used as mask to transfer the same pattern into the SiO_2 layer.

The SiO_2 film is etched using a Plasma Therm Reactive Ion Etcher (RIE) in the NanoStructures Lab (NSL). In a reactive ion etcher, a reactive gas species is added to the chamber. When a plasma is formed by the applied rf potentials, the electrons collide with the gas molecules causing dissosciation of the molecules into a number of fragments and radicals. A significant number of these molecular fragments become

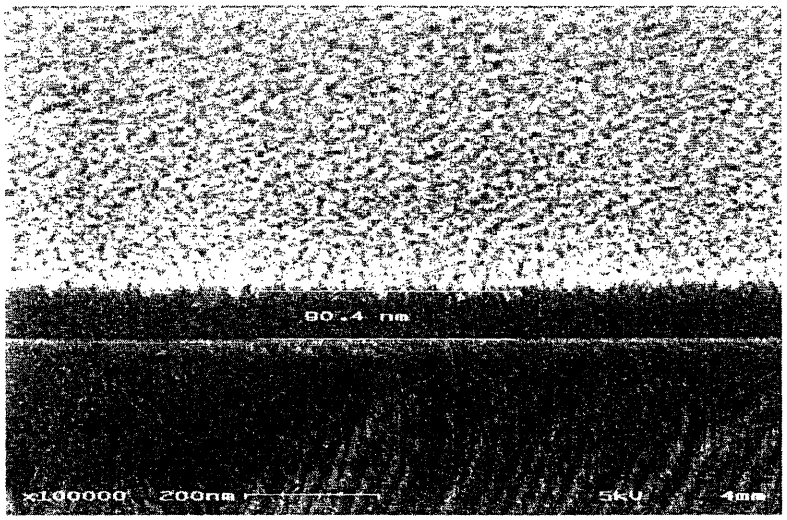

Figure 3-5: Cross section of the oxide film through a SEM

ionized in the plasma and are accelerated to the various electrode surfaces within the discharge chamber. The samples are placed on the powered electrode and exposed to the flux of ions from the plasma. During reactive ion etching, gaseous species from the plasma react with the surface atoms forming compounds or molecules. These species then leave the surface either thermally or as a result of ion bombardment. For the etching of the SiO_2 layer, CHF_3 gas was used as the reactive gas species. After etching the SiO_2 layer, the photo resist layer is removed by ashing which involves oxidation of the resist to form a volatile compound. Figure 3-5 shows a cross-section of the etched oxide film as seen through a Scanning Electron Microscope (SEM). The SiO_2 thickness measured using SEM is 90.4 nm. The oxide mask formed using the above procedure is then used to etch the InGaP/InGaAlP layers of the structure. The III-V layers are etched using a $CH_4 : H_2 : O_2$ mixture in a parallel plate RIE system in the NSL.

3.2.3 Oxidation

The DBR test structure containing alternating layers of AlAs and InGaAlP was oxidized to convert the AlAs layers to low dielectric constant Al_xO_y. A wet thermal oxidation process was used. In this process oxygen is provided by passing water vapor

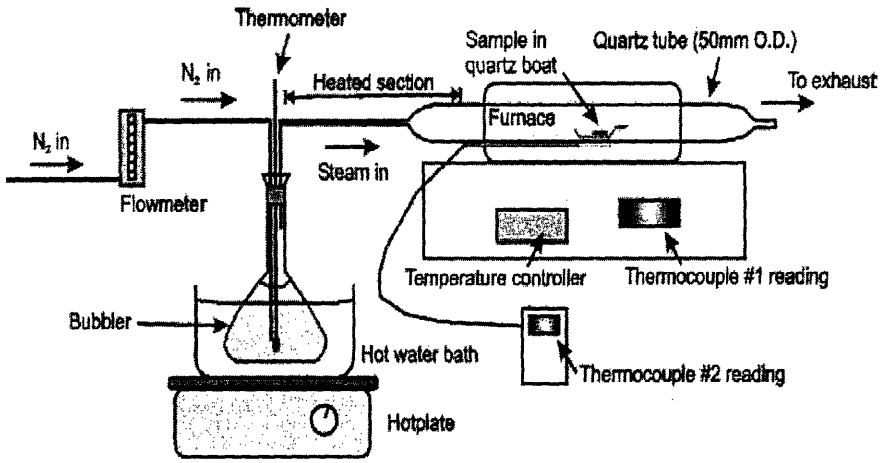

Figure 3-6: Schematic of the oxidation set up

over the sample to be oxidized. The oxidation set up (Figure 3-6) consists of a quartz tube placed in a furnace which is maintained at 410 degree C. N_2 gas flows over a DI H_2O bubbler heated to 90 degree C and carries water vapor through the quartz tube. The quartz boat is heated inside the furnace until the temperature stabilizes. The quartz boat is then removed from the furnace and replaced with the sample on the boat. The rate of nitrogen gas was kept constant at 1.5 liters/min. A 0.5 cm x 0.5 cm sample was oxidized for 2 hours with a 50 minute ramp up time. The microscopic image of the sample after oxidation is shown in Figure 3-7. The oxidized edge of the sample can be seen in a different color in the image. The small oxidized circles seen in the sample are defects.

3.3 Characterization

3.3.1 Photoluminescence

The emission spectrum of all the quantum well structures was measured using room temperature photoluminescence (PL). Figure 3-8 shows the PL plot obtained for the quantum well structure with a single quantum well of 6 nm thickness. The sample is

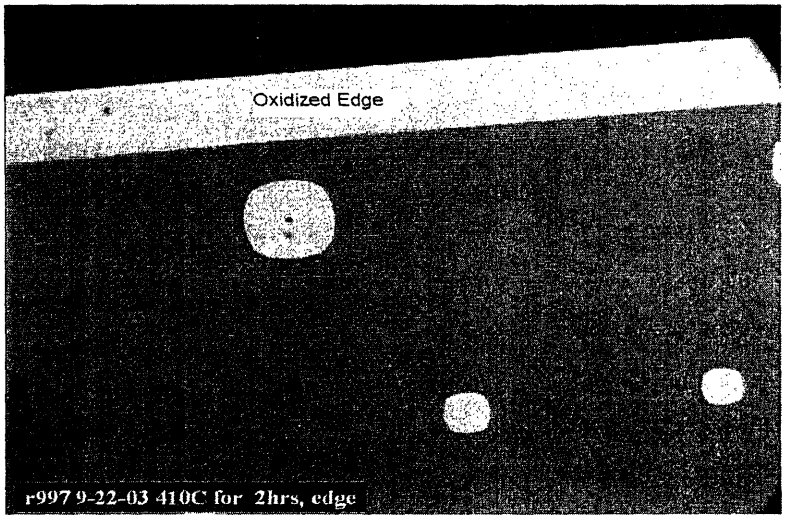

Figure 3-7: Microscopic image of the oxidized edge of the sample

pumped using an argon laser emitting at a wavelength of $\lambda = 488nm$. The emitted light is focused into a spectrometer and analysed using a Si detector. The scanning range used was 500 to 710 nm and the sensitivity was 2 mV. As seen from the plot in Figure 3.8, the peak wavelength of emission obtained for this structure was 647.5 nm. The full-width-half-maximum (FWHM) for this structure was found to be 18 nm. PL measurement was also carried out for the 690 nm device which contains both the multi-quantum well structure and the DBR. A photomultiplier tube was used as the detector for the PL measurement of the 690 nm device. The scanning range used was 600 to 800 nm and a sensitivity of 500 mV was used. Figure 3-9 shows the emission spectrum obtained for this device. Two peaks at wavelengths of 686 nm and 725 nm were obtained. The two peaks could be due to the misalignment of the reflectance peak and the quantum well emission peak with each other. A more detailed discussion on the PL spectra in Figure 3.9 is presented in Chapter 4.

3.3.2 Reflectivity measurements

Reflectivity measurements were performed on the distributed bragg reflectors (DBRs). The DBR made without oxidation was measured using the Absolute Specular Reflectance accessory of the Cary 5E UV-Vis-NIR Dual-Beam Spectrophotometer. The

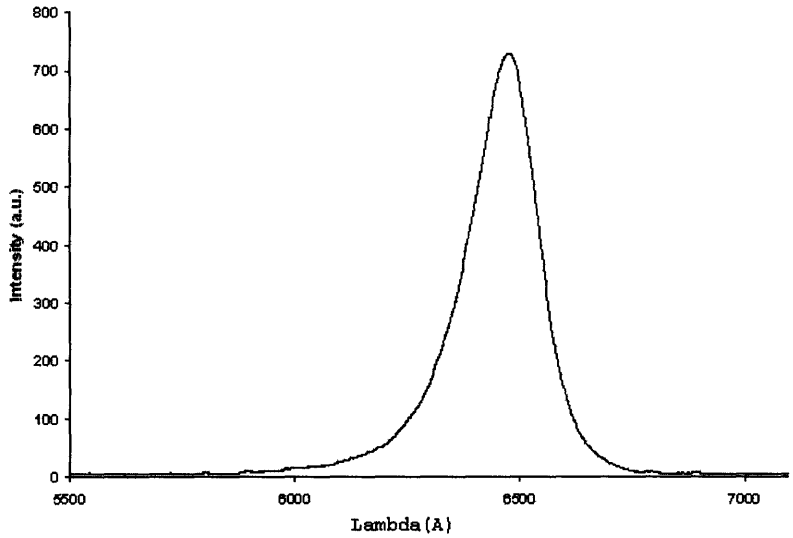

Figure 3-8: PL from 6 nm InGaP/InGaAlP quantum well structure

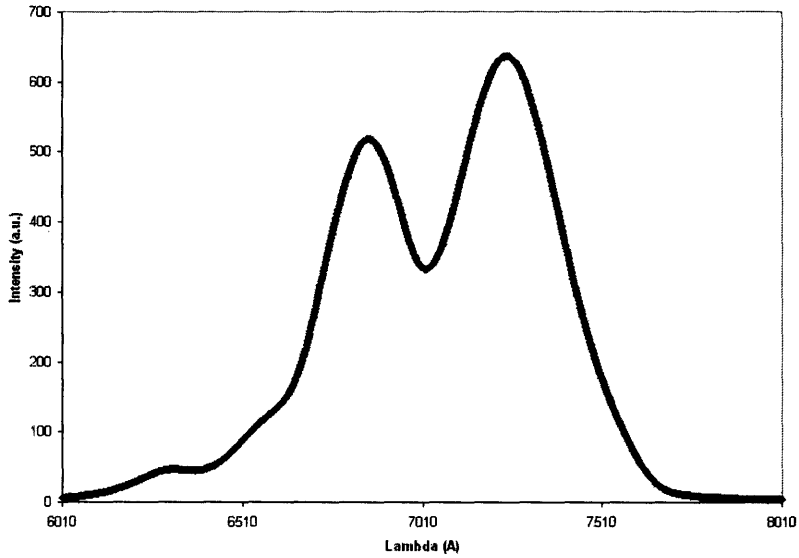

Figure 3-9: PL spectra from InGaP/InGaAlP multi quantum well structure with AlGaAs/AlAs DBR

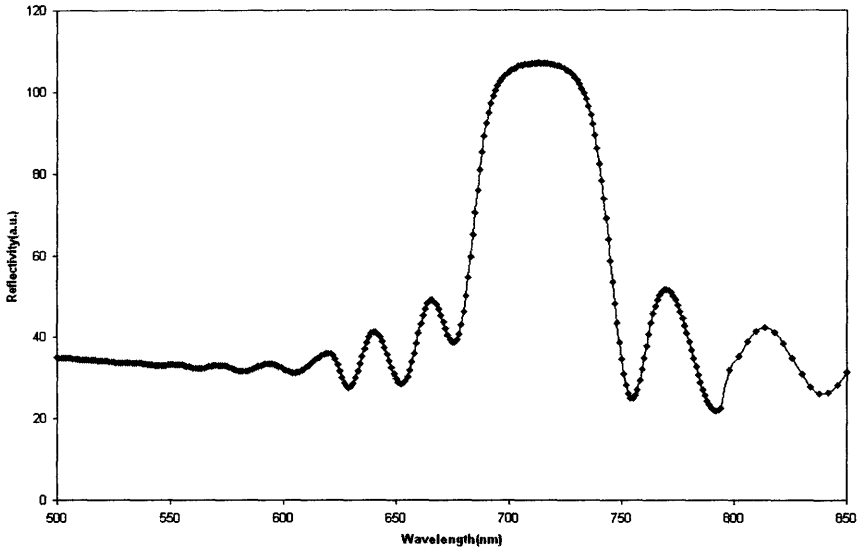

Figure 3-10: Reflectivity versus wavelength measured for AlGaAs/AlAs DBR

DBR was made using alternate layers of AlGaAs and AlAs. The sample was scanned using wavelengths ranging from 500 nm to 800 nm to obtain the range of wavelength with high reflectance. Figure 3-10 shows the reflectivity versus wavelength plot for this DBR. As seen from this figure, the highest reflectivity is obtained at a wavelength of 713 nm.

Reflectivity measurements were also done on the oxide DBR formed at the edges of the oxidized sample. This was done using a QDI 1000 UV-Visible NIR Reflectance Microspectrophotometer by Craic Technologies. The reference material used was a bare Silicon wafer. Figure 3-11 shows the reflectance spectra obtained at various locations in the oxidized sample. Location 1 in Figure 3-11 refers to the oxidized edge of the sample and location 2 refers to the unoxidized area. As seen from the figure, a very high reflectivity is obtained at wavelengths greater than 600 nm for the oxide DBR formed at the edge. Due to the large range of wavelength showing high reflectivity, the DBR possesses a wide stop band. The unoxidized part of the sample shows low reflectivity in addition to a high level of interference.

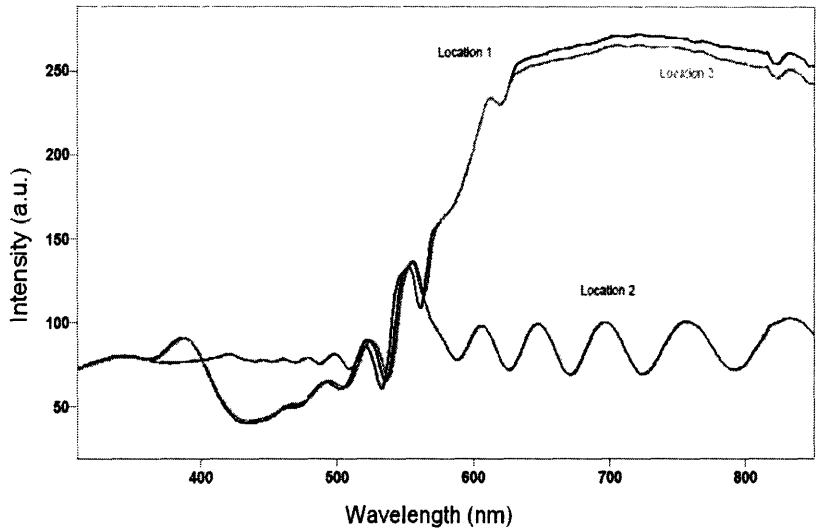

Figure 3-11: Reflectivity versus wavelength measured for InGaAlP/AlxOy DBR [13]

3.3.3 X-Ray diffraction analysis

X-ray diffraction was used to characterize the layers in the 650 nm emitter structure. Figure 3-12 shows a plot of the measured x-ray diffraction curve as a function of the angle theta. Each peak represents the diffracted intensity from an individual layer. Theta represents the angle between the detector and the wafer. The experimental x-ray curve is compared to the simulated x-ray diffraction curve to determine the thickness and composition of the various layers in the structure.

In the x-ray diffraction curve, the position of the diffracted peaks shifts in theta with different layer compositions. Thus alignment of the peaks of a simulated curve with specified layer composition to that of the measured curve determines the composition of the layers in the as-grown device structure. The substrate peak has known composition (GaAs) and is the most intense diffracted peak. Thus the experimental diffracted peak is aligned with the simulated substrate peak first. Both peaks are then offset to theta=0. The composition of the other layers is then determined by matching other peaks.

The width of a simulated peak varies with the thickness of the corresponding layer. A thicker layer corresponds to a thinner peak and vice versa. From the plot in

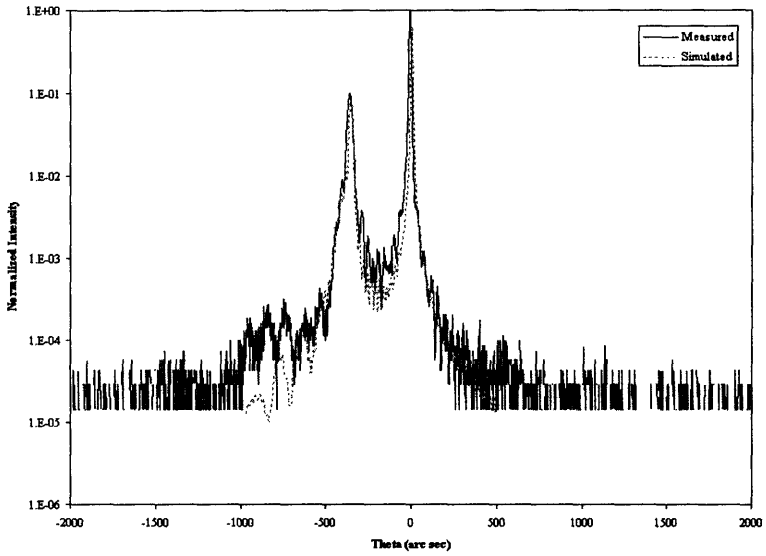

Figure 3-12: Plot of measured X-ray diffraction curve

Figure 3-12, it is found that the grown layers in the structure are not exactly lattice matched to the GaAs substrate as desired. The second intense peak seen in the figure is from the AlGaAs layer which is about 350 arc seconds from the GaAs layer. The composition of the AlGaAs layer was found to be 93% AlAs and 7% GaAs and its thickness was found to be 660 nm. The thickness and composition of the InGaP quantum well and the InGaAlP cladding layer could not be accurately determined due to slight imperfect alignment in the smaller peaks.

Chapter 4

Discussion

4.1 Photoluminescence of InGaP quantum well calibration structure

A quantum well calibration structure consisting of two InGaP quantum wells with different thicknesses was grown. The thicknesses of the quantum wells were 2 nm and 6 nm. InGaAlP was used as both the barrier and the cladding layer for the quantum wells. Photoluminescence spectrum due to this quantum well structure was measured at room temperature and is shown in Figure 4-1. Since the structure consists of two quantum wells, 2 peaks are expected in the PL plot. As seen from Figure 4-1, a single peak at 642 nm was observed using room temperature PL measurement. Low temperature PL at 10 K was performed and the emission spectra obtained is shown in the plot in Figure 4-2. The plot shows 2 peaks corresponding to the two different quantum wells. The difference in the PL spectra obtained at room temperature and at 10 K is explained below. For a thin quantum well, the energy levels inside the quantum well are present farther away from the band edges of the quantum well material. Thus the energy levels for 2 nm thick quantum well are closer to the band edge of the barrier or cladding layer resulting in a very low energy difference between the quantum wells states and the band edges of the cladding layer. Hence at room temperature, carriers have enough thermal energy to jump from the quantum well to

the cladding layer and hence does not result in confinement of the charge carriers. Thus only a single peak corresponding to the 6 nm thick quantum well is observed at room temperature. At low temperatures (close to 10K), the thermal energy of the charge carriers is not sufficient for transition from the quantum well states to the cladding layer states. Thus the charge carriers are confined in the quantum well and light emission is obtained as a result of recombination of those charge carriers. Thus two peaks corresponding to both the 2 nm and the 6 nm quantum wells are observed using PL at 10 K. The peak corresponding to the 2nm quantum well is observed at lower wavelength since the energy states for the thinner quantum well are farther apart and hence greater energy is released as a result of recombination.

The emission spectrum obtained using PL at 10K was compared with a particle in a box calculation for the energy states of the quantum well structure. The electron and hole energy states were calculated using Equation 4.1 for quantum well states in a finite square well potential.

$$E_n + V_0 = n^2h^2/8m^*L^2 \tag{4.1}$$

In the above equation, $E_n + V_0$ is the energy above the bottom of the well, m^* is the effective mass of the electron or hole and L is the thickness of the quantum well. The band gap of InGaP was calculated using linear interpolation of band gaps of InP and GaP. The recombination energy of electrons and holes is given by the sum of the band gap of the quantum well and the energies of electrons and holes above the bottom of the well. Comparing the room temperature PL emission obtained at 642 nm with the recombination energy, the band gap of InGaP was found to be 1.855 eV which corresponds to the composition $In_{0.65}Ga_{0.35}P$ for the quantum well. At 10K the band gap of $In_{0.65}Ga_{0.35}P$ is calculated to be 1.926eV. Using 1.92eV for band gap in the calculation of recombination energy at 10K and comparing with the 570nm peak observed in PL at 10K, the thickness of the thinner quatum well was found to be 3.4nm. The wavelength of emission corresponding to the 6nm quatum well at 10K was calculated to be 619nm which is close to the observed peak in PL at 10K (shown in Figure 4-2). The electron energy state in a 3.4nm thick quantum well was

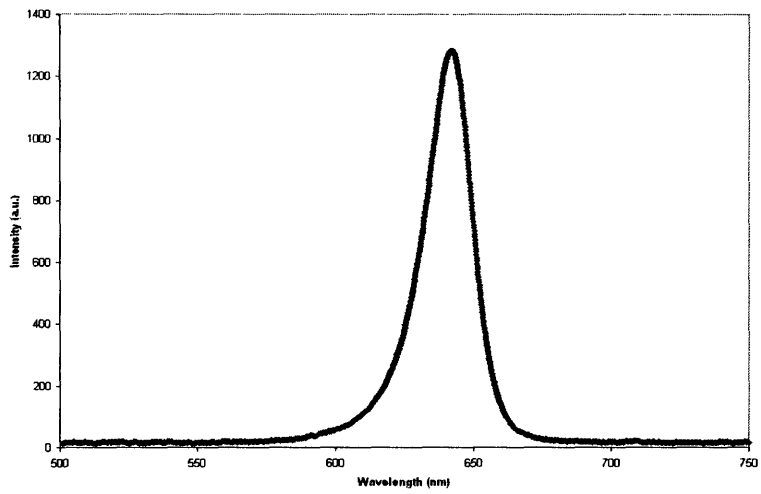

Figure 4-1: Room temperature PL spectra from InGaP/InGaAlP calibration structure

calculated (using Equation 4.1) to be 0.203eV. The conduction band offset for the quantum well at room temperature was calculated to be 0.19eV. Thus the energy state for the thinner quantum well is not confined at room temperature. This is in agreement with the PL result at room temeperature which shows only a single peak corresponding to the thicker quantum well.

4.2 Distributed bragg reflectors

Two different distributed bragg reflector (DBR) structures were presented in this thesis. The first structure consisted of alternating layers of InGaAlP/AlxOy. AlxOy was formed by oxidation of AlAs layers. As described in section 3.3.2, the oxide DBR possessed a wide stop band ranging from wavelengths of 600 nm to 850 nm. Thus this structure could be used as a DBR for any device structure emitting in the red and near infra-red region of the electromagnetic spectrum. Thus it is easier to hit the target design with this DBR structure compared to ones with narrow range of high reflectivity. On the other hand fabrication of large area devices for this design is difficult due to the slow oxidation rate (0.5 micron per minute). In addition delamination of films has been observed for large area oxidized DBRs due

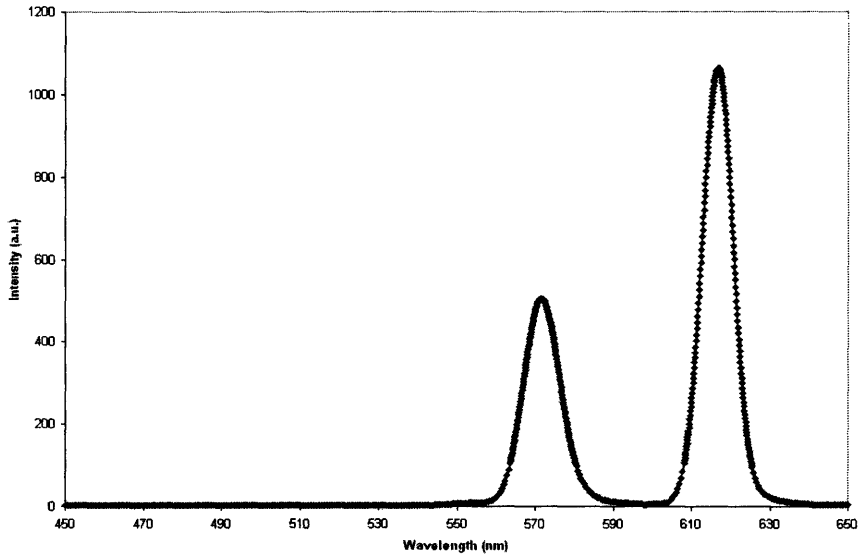

Figure 4-2: PL spectra from InGaP/InGaAlP calibration structure at 10 K

to contraction when AlAs is converted to AlxOy [1].

The second DBR structure presented in this thesis consisted of alternating layers of AlAs/AlGaAs. Due to the low index contrast between AlAs and AlGaAs, this DBR requires more number of layers (16) compared to the oxide DBR which required only 7 bilayers. This non-oxidized DBR possessed a very narrow stop band (40 nm) and thus results in less robustness. The AlAs/AlGaAs DBR can hence be used as a mirror for only a small range of wavelengths. However the AlAs/AlGaAs DBR has the advantage of ease of fabrication over the oxide DBR mentioned above. Since the AlAs/AlGaAs DBR does not require oxidation, large area DBRs can be fabricated using this design and is also not prone to delamination.

Another interesting feature of the the AlGaAs/AlAs DBR was the radially symmetric reflectance distribution across the wafer. The AlGaAs/AlAs DBR was grown on a 2 inch diameter wafer and reflectance measurements were done at several points along the diameter of the wafer. Figure 4-3 shows the reflectance spectra measured for points along the radius of the wafer moving from the edge toward the center of the wafer. As seen from Figure 4-3, the peaks in reflectivity shift toward lower wavelengths as we move from the center to the edge of the wafer. The reflectivity peak is

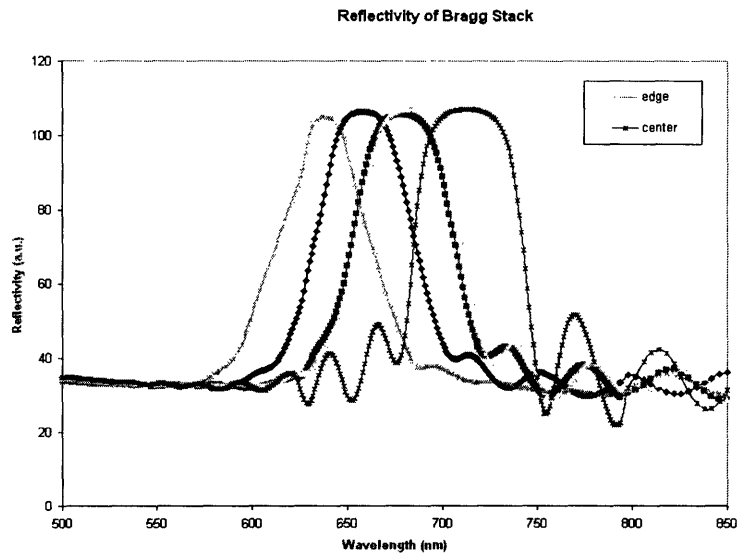

Figure 4-3: Reflectance data along the radius of the wafer containing AlGaAs/AlAs DBR

centered around 713 nm for the center of the wafer whereas for the edge of the wafer the reflectivity peak is centered around 635 nm. The geometry of the sources and the substrate position in the reactor of the MBE results in slight variation in growth conditions along the radius of the wafer and hence a radially symmetric reflectance data measured across the wafer.

4.3 Photoluminescence results for 690 nm emitter structure

The photoluminescence spectra obtained for the 690 nm device structure which contains both the multi quantum well active region and the DBR is shown in Figure 4-4. As seen in the figure, the PL spectra contains two peaks instead of a single peak at around 690 nm. According to the design, both the multi quantum well structure and the DBR should emit and reflect respectively at 690 nm. Thus the emission peak due to the multi quantum well structure and the reflectance peak due to the DBR was expected to overlap and give rise to a single peak around 690 nm. The two

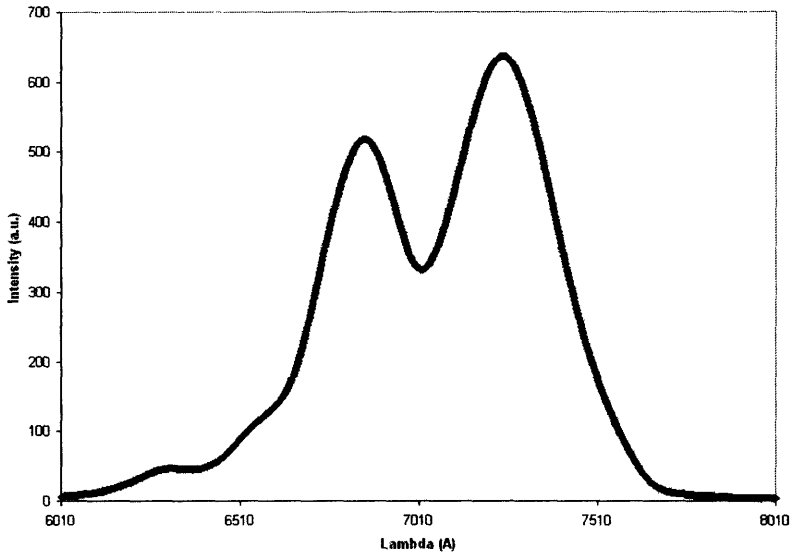

Figure 4-4: PL spectra from the structure containing both InGaP/InGaAlP multi quantum well active region and the AlGaAs/AlAs DBR

peaks seen in Figure 4-4 could be a result of the mismatch between the emission and the reflectance peak. Figure 4-5 shows the normalized emission spectra of just the quantum well structure and the normalized reflectance spectra of the DBR on the same graph. It can be seen from this figure that the superposition of the emission and the reflectance spectra would result in the PL spectra obtained for the complete device structure (shown in Figure 4-4). The peak at higher wavelength can be due the reflectance peak of the DBR where as the peak at lower wavelength could be due to the quantum well structure. The dip between the two peaks could be a result of the abrupt drop in reflectivity at those wavelengths.

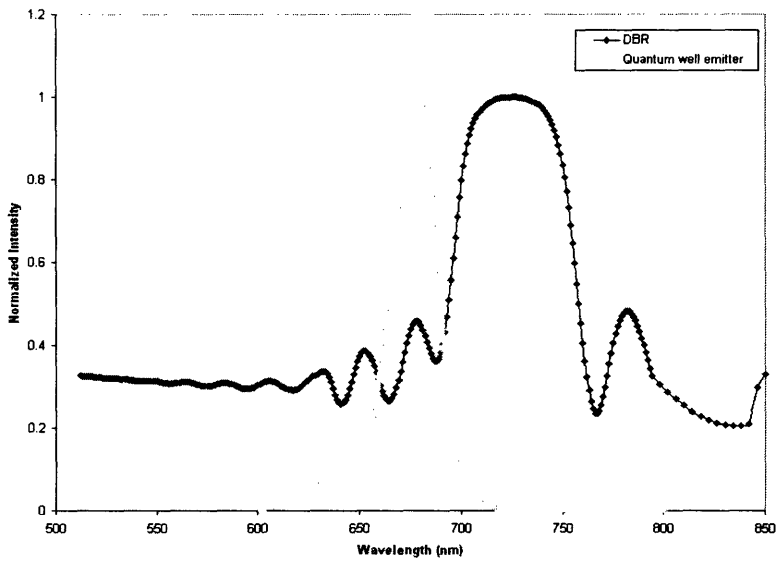

Figure 4-5: Plot showing the PL spectra of the multi quantum well emitter and also the reflectance spectra of the AlAs/AlGaAs DBR. Normalized intensities are plotted in both cases.

Chapter 5

Conclusions and future work

5.1 650 nm emitter

A quantum well active region emitting at a peak wavelength of 648 nm and FWHM of 18 nm was successfully grown and tested using photoluminescence (PL) measurements. The active region consisted of InGaP quantum well and InGaAlP cladding layer. A distributed bragg reflector (DBR), designed for strong reflectivity at 650 nm was also successfully fabricated and tested. The DBR consisted of alternate layers of aluminum oxide and InGaAlP.

5.1.1 Future work

Future work would involve integrating the DBR and the quantum well active region for the 650 nm device. This would involve growth of the entire structure in a single growth process, patterning of the as-grown wafer into small mesas and oxidation of the mesas to form the oxide layer in the DBR. Since the DBR for the 650 nm structure contained an oxide layer, only small area devices containing this DBR can be made. Alternate DBR structures that would not require oxidation may be designed for strong reflection at 650 nm. Photonic Crystal LEDs have shown to possess higher extraction efficiencies. A large amount of emitted light is reabsorbed due to total internal reflection at the dielectric interface. A photonic crystal eliminates guided

modes of frequencies lying within the band gap of that photonic crystal and hence the emitted light is forced to couple to radiation states leading to higher efficiencies. Thus the efficiency of the device can be increased by etching a photonic crystal with appropriate photonic band gap in the top cladding layer.

5.2 690 nm emitter

A red emitting device which integrates a multi-quantum well active region and a DBR has been fabricated using molecular beam epitaxy. The active region was grown using InGaP/InGaAlP material system and the DBR was made using alternate layers of AlGaAs and AlAs. Testing of the entire device structure using photoluminescence resulted in two peaks instead of a single peak at 690 nm. Both the multi-quantum well emitter and the DBR have been independently grown and tested using PL and reflectance measurements respectively. PL on the multi-quantum well emitter results in a peak at the desired wavelength. Reflectance measurement on the DBR showed the reflectivity peak to be shifted to a higher wavelength than desired. The stop band of the DBR was found to be approximately 40 nm. In addition, reflectance measurements across the wafer of the DBR revealed a radially symmetric distribution of reflectivity across the wafer.

5.2.1 Future work

The reflectivity data obtained from the DBR should be verified by growing and testing more identical DBR structures. In order to obtain a single peak from the integrated quantum well and DBR structure, the reflectivity peak from the DBR should be shifted to lower wavelengths (close to 690 nm). Hence the thickness and/or composition of the DBR layers should be changed slightly to obtain strong reflectivity at 690 nm. DBR structures with different design should also be attempted to obtain a wide stop band. A wide stop band would result in a more robust design. With a wide stop band, slight variations in growth conditions will still result in strong reflectivity at the desired wavelength.

Hybrid organic-inorganic devices are an active area of current research as they open up the possibility of combining the advantages of both organic and inorganic semiconductors. Since the emission wavelength (690 nm) of the device presented in this thesis, overlaps with the absorption peak of J-aggregate cynanine dye (an organic semiconductor), the 690 nm emitter should be integrated with the organic semiconductor J-aggregate cynanine. The integrated organic-inorganic device will yield more insight into the field of hybrid organic-inorganic devices.

Bibliography

[1] Alexei A. Erchak *Enhanced Performance of Optical Sources in III-V Materials Using Photonic Crystals* 2002, Doctor of Philosophy Thesis, Massachusetts Institute Of Technology.

[2] S. R. Forrest *Nature*, 2004 , Vol. 428, No. 6986, 911-918.

[3] S. R. Forrest *IEEE Circuits and Devices Magazine*, 1989, Vol. 5, p33.

[4] Bahaa E. A. Saleh and M. C. Teich *Fundamentals of Photonics* 1991.

[5] E. H. C. Parker *The Technology and Physics of Molecular Beam Epitaxy* 1985: Plenum Press, New York.

[6] M. B. Panish and H. Temkin *Gas Source Molecular Beam Epitaxy* 1993: Springer-Verlag, Berlin.

[7] Instruction Manual for High Temperature Gas Cell, Riber Division d'Instruments S.A., 1990.

[8] M. A. Herman and H. Sitter *Molecular Beam Epitaxy* 1989: Springer-Verlag, Berlin.

[9] Elisabeth M. Koontz *The development of Components for Ultrafast All-Optical Communications Networks* 2000, Doctor of Philosophy Thesis, Massachusetts Institute Of Technology.

[10] D. K. Bowen and Brian K. Tanner *High Resolution X-ray Diffractometry and Topography* 1998: Harvard University Press.

[11] Information Bulletin for Bede D^3 x-ray characterization system, Bede Scientific Instruments Ltd., Durham U.K.

[12] User guide for Specular Reflectance Accessory, Varian Inc.

[13] Sample Analysis Report for Microspectral Analysis of InGaAlP/AlxOy Distributed Bragg Reflectors, Craic Technologies, 2003.